Enhanced Room-Temperature Geometric Magnetoresistance in Inhomogeneous Narrow-Gap Semiconductors

S. A. Solin,[1]* Tineke Thio,[1] D. R. Hines,[1] J. J. Heremans[2]

A symmetric van der Pauw disk of homogeneous nonmagnetic indium antimonide with an embedded concentric gold inhomogeneity is found to exhibit room-temperature geometric magnetoresistance as high as 100, 9100, and 750,000 percent at magnetic fields of 0.05, 0.25, and 4.0 teslas, respectively. For inhomogeneities of sufficiently large diameter relative to that of the surrounding disk, the resistance is field-independent up to an onset field above which it increases rapidly. These results can be understood in terms of the field-dependent deflection of current around the inhomogeneity.

Magnetoresistive sensors are critical components in technologies such as high-density information storage (*1*) and position/speed monitoring in mechanical devices (*2*, *3*). The magnetoresistance (MR) of such sensors contains a physical contribution from the magnetic field dependence of the material parameters and a geometric contribution from the dependence of the current path and output voltage on the sample shape and electrode configuration (*4*, *5*). Either the physical or geometrical contribution may dominate the observed MR. To date, only two classes of magnetic materials, artificially layered metals (*6*) and the manganite perovskites (*7*), which exhibit giant MR (GMR) (*8*) and colossal MR (CMR) (*9*), respectively, have been considered serious candidates in the drive to develop sensors with increased MR at room temperature (RT). For both of these classes, the physical MR dominates. In contrast, we found that patterned nonmagnetic InSb, a high-mobility narrow-gap semiconductor, exhibits RT enhanced geometric MR orders of magnitude larger than the physical MR obtained to date with other materials.

In layered metals or manganite perovskites, the MR is negative (the resistance decreases with applied magnetic field), whereas the MR of a nonmagnetic semiconductor is positive and usually includes physical and geometric contributions (*10*). In such materials, the physical MR results from the orbital motion of the charge carriers caused by the Lorentz force. So does the geometric MR, but it also depends strongly on the boundary conditions for current flow. The geometric MR increases quadratically with mobility and magnetic field at low field (*5*); therefore, high-mobility narrow-gap semiconductors (*11*), such as InSb and $Hg_{1-x}Cd_xTe$, are attractive materials for exploring geometric effects. Inhomogeneities can enhance the geometric MR of a material (*12*, *13*), but such enhancements have been rather small, typically less than a factor of ~20 change in resistance in a magnetic field of H-1 T (*13*, *14*). The much larger changes that we report result from current deflection by the inhomogeneity that approximates a short circuit at zero magnetic field and an open circuit at high field.

Our samples consist of metal organic vapor phase epitaxy-grown epilayers of Te-doped n-type InSb. A buffer layer of 200-nm undoped InSb was grown on a 4-inch semi-insulating (100) GaAs substrate (resistivity > 1×10^{15} ohm·m). A 1.3-μm active layer of InSb (electron concentration $n = 2.6 \times 10^{22}$ m^{-3} and mobility $\mu = 4.55$ m^2/Vs) was deposited on the buffer layer and capped by a 50-nm InSb contacting layer ($n \sim 1.5 \times 10^{23}$ m^{-3}). This epitaxial sequence was passivated by a 200-nm layer of Si_3N_4. Because of lattice mismatch at the GaAs/InSb interface, the in-plane RT mobility of InSb drops rapidly with thickness below ~1 μm (reaching a value of 0.1 m^2/Vs at 150 nm (*15*). Thus, the InSb buffer does not represent a parallel conduction channel. The heavily doped thin cap layer has low mobility and is partially depleted because of band-bending at the $InSb/Si_3N_4$ interface. Hence, this layer likewise does not contribute to parallel conduction. The wafers were photolithographically patterned into chips bearing mesas (Fig. 1, inset). The circular mesas (diameter = 1 mm) contain four equally spaced contact pads and a concentric hole with smooth side walls (average wall angle ~19° from vertical, tapered outward), prepared by reactive ion etching. Subsequently, the hole and mesa contact pads were simultaneously metalized with a Ti/Pt/Au stack, with Au the dominant component, forming a modified van der Pauw (vdP) geometry. Contacting was by wire-bonding.

The MR was therefore measured with a concentric conducting inhomogeneity of radius r_a and conductivity σ_0 (= 4.52×10^7/ohm·m for Au) embedded in a vdP disk of homogeneous semiconductor of radius r_b and conductivity σ (= 1.86×10^4/ohm·m for InSb) $\ll \sigma_0$. This construct was first used by Wolfe *et al.* (*16*) to account theoretically for geometrically induced mobility and Hall coefficient anomalies exhibited by inhomogeneous semiconductors. We define two parameters, the filling factor $\alpha = r_a/r_b$ and the conductivity ratio $s = \sigma_0/\sigma$. Then, for fixed current, i, the effective four-contact resistance of the composite disk is $R(H,T,\alpha,s) = V(H,T,\alpha,s)/i$, where V is the measured voltage (Fig. 1) and T is the temperature. We report here only RT measurements with Au inhomogeneities in InSb so we drop the temperature and s variables and define the MR as $[\Delta R(H,\alpha)]/R_0^{\alpha} = [R(H,\alpha) - R_0^{\alpha}]/R_0^{\alpha}$, where now $R_0^{\alpha} = R(0,\alpha)$. The standard vdP geometry (*5*) corresponds to the case $\alpha = 0$. (Normally, a vdP measurement of the sheet resistance, or

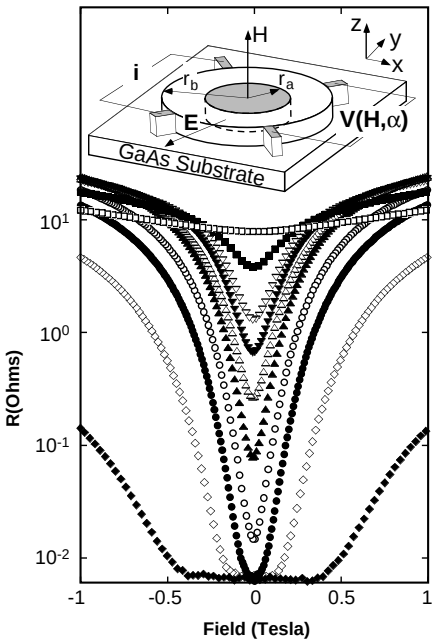

Fig. 1. The RT resistance up to 1 T of a composite vdP disk of InSb and Au for a number of values of $\alpha = r_a/r_b$. The symbols correspond to 16α = 0, □; 6, ■; 8, ▽; 9, ▼; 10, △; 11, ▲; 12, ○; 13, ●; 14, ◇, and 15, ◆. (**Inset**) A schematic diagram of a cylindrical Au inhomogeneity (radius r_a) of conductivity σ_0 embedded in a homogeneous InSb vdP disk (radius r_b) with conductivity σ. The electric field **E** is normal to the interface between the semiconductor and inhomogeneity. The vector **H** represents a uniform magnetic field in the z direction. The vdP disk and equally spaced contact pads are formed as an etched mesa. The wiring configuration shown applies to the measurement of MR.

[1]NEC Research Institute, 4 Independence Way, Princeton, NJ 08540, USA. [2]Department of Physics and Astronomy, Ohio University, Athens, OH 45701, USA.

*To whom correspondence should be addressed. E-mail: solin@research.nj.nec.com

equivalently, the resistivity, requires two voltage measurements from different pairs of current and voltage electrodes. For the four-fold symmetric geometry used here, only one such measurement is required.)

A semilog plot of $R(H,\alpha)$ for $0 \leq H \leq 1$ T and for various values of α from 0 to 15/16 (Fig. 1) shows that $R(0,\alpha)$ drops monotonically with increasing α as a result of the increasing conductance of the inhomogeneity. However, because the conductivity of the Au inhomogeneity is finite, $R(0,\alpha)$ saturates at large $\alpha > \sim 13/16$. We took care to verify that this saturation is real and not an artifact of the measurement apparatus. When saturation occurs, the resistance becomes field-independent up to a critical field above which it rises rapidly with increasing field. Thus, for sufficiently large α, the device acts like a magnetic diode or switch.

The MR dependence on α for a family of fixed magnetic fields (Fig. 2) shows that it grows monotonically up to $\alpha = 12/16$ or 13/16, above which it precipitously decreases. Also note (Fig. 3) that the MR evolves from a quadratic to a quasi-linear field dependence up to $\alpha = 13/16$, and for fields above $\sim$2 T, it either saturates or, for $\alpha = 14/16$ and 15/16, exhibits a maximum. However, the most notable feature of the data of Figs. 2 and 3 is the magnitude of the MR. For $\alpha = 12/16$, the MR is 113% at 0.05 T, whereas for $\alpha = 13/16$, it is 9100% at 0.25 T and 750,000% at 4 T. For comparison, we note that layered metals exhibit a GMR of $\sim$22% at RT and 0.005 T (*8*) or giant magnetotunneling of $\sim$42% at RT and 0.0003 T (*17*), whereas the manganite perovskites (*7*) show a CMR of 127,000% at 77 K and 6 T but only 39% at RT and 1.75 T (*9*).

To discuss the principles (*16*, *18*) that underlie the achievement of such high values of RT MR, we consider the composite vdP geometry. The components of the magnetoconductivity tensor $\boldsymbol{\sigma}(H)$ for the semiconductor are $\sigma_{xx}(\beta) = \sigma_{yy}(\beta) = \sigma/[1 + \beta^2]$, $\sigma_{zz}(\beta) = \sigma$, and $\sigma_{xy}(\beta) = -\sigma\beta/[1 + \beta^2] = -\sigma_{yx}(\beta)$ with $\beta = \mu H$. All other tensor components vanish. The electric field, **E,** is normal to the equipotential surface of the highly conducting inhomogeneity. The current density is written as $\mathbf{J} = \boldsymbol{\sigma}(H)\mathbf{E}$. At $H = 0$, $\sigma(H)$ is diagonal so $\mathbf{J} = \sigma\mathbf{E}$ and the current flows into the inhomogeneity, which acts as a short circuit. At high H ($\beta > 1$), the off-diagonal components of $\boldsymbol{\sigma}(H)$ dominate so $\mathbf{J} \perp \mathbf{E}$. Equivalently, the Hall angle (*5*) between **E** and **J** approaches 90°, and the current becomes tangent to, i.e., deflected around, the inhomogeneity. Thus, the inhomogeneity acts as an open circuit. The transition of the inhomogeneity from short circuit at low H to open circuit at high H results in a geometric enhancement of the MR of the semiconductor even if its physical MR is zero. The geometric MR increases with α because R_0^{α} decreases. However, when α becomes sufficiently large so that the low-field current flows mostly through the inhomogeneity, the MR will be that of the inhomogeneity itself, which for Au is negligibly small. Then an appreciable MR is only observed when H is sufficient to deflect the current from the inhomogeneity such that the conductance through the metallic inhomogeneity is smaller than the conductance through the semiconductor annulus of thickness $r_b - r_a$.

It is instructive to compare the underlying mechanism of the enhanced MR geometry with that of other four-terminal devices (Hall geometry) and with two-terminal geometrical magnetoresistors (Corbino geometry). In this comparison, we define R as V/i, where V is a voltage measured over two contacts in response to a current applied to the same or different contacts. For all three geometries, the H dependence of R results from the existence of field-dependent off-diagonal components in the conductivity tensor and from the boundary conditions of the structure. However, the enhanced MR geometry is unique by virtue of the boundary condition imposed by the inhomogeneity. The Hall geometry differs from the Corbino and enhanced MR geometries by the symmetry of $R(H)$: The Hall response is antisymmetric and linear; hence, $R_{Hall}(H = 0) = 0$. In contrast, both MR geometries exhibit a resistance that is symmetric in H and quadratic at low H with $R_{MR}(H = 0) \neq 0$. Thus, enhanced geometric MR devices can be directly compared with Corbino devices and also with other two-terminal devices operating on physical MR principles. The definition of MR, as $[R(H) - R(H = 0)]/R(H = 0)$, is not applicable to devices exhibiting antisymmetric behavior (Hall), because in those cases $R(H = 0)$ is necessarily zero. Therefore, despite its four-contact character, the enhanced MR effect must be differentiated from the Hall effect.

The approximately quadratic behavior of enhanced MR for $\alpha \leq 13/16$ at low H allows us to apply the form $[\Delta R(H,\alpha)]/R_0^{\alpha} = \{\mu_{app}^{\alpha}(H - H_0)\}^2$, where μ_{app}^{α} is the apparent mobility (*18*) and H_0 is a small zero-field offset (*19*). The apparent mobilities obtained from fits to the data with the use of this form are larger than the actual mobility of the semiconductor. Indeed, for $\alpha = 13/16$, we find $\mu_{app}^{13/16}/\mu = 22.3$. The quasi-linear response and roll off of the MR at higher fields can also be quantitatively accounted for by use of an augmented Wolfe model that we have used previously (*18*) to explain the much smaller MR that results from natural growth-induced microscopic inhomogeneities in $Hg_{1-x}Cd_xTe$, $x = 0.1$. The application of this model to the enhanced MR of InSb is addressed elsewhere (*20*).

A comparison of the expected performance of enhanced MR devices with other magnetic sensors in common use is also appropriate. Such a comparison is facilitated by considering the high-frequency (>100 kHz) power signal-to-noise ratio (SNR) for which thermal noise is dominant. It can be shown that for an enhanced geometric MR sensor and a Hall sensor of the same (homogeneous) material and approximately equivalent dimensions, SNR_{MR}/SNR_{Hall} is proportional to μ_{app}/μ (*5*, *21*). Thus, our enhanced geometric MR devices should be superior to Hall sensors. Consider now two-probe metallic physical GMR sensors. As SNR_{MR} is proportional to $(\Delta\rho/\rho)^2\rho$ (*21*), the two-probe advantage is

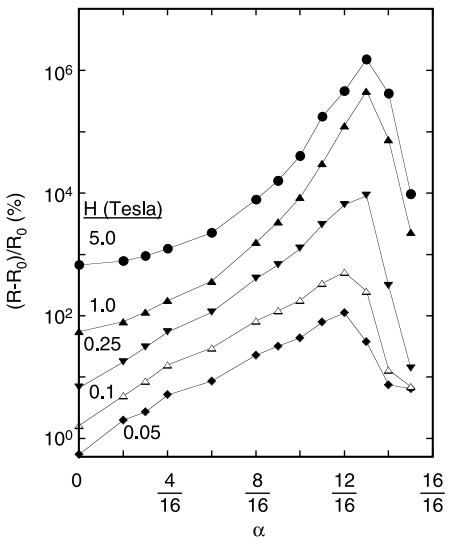

Fig. 2. The RT MR versus filling factor, α, of a composite vdP disk of InSb and Au for several values of magnetic field. The symbols correspond to $H = 0.05$ T, ◆; 0.1 T, △; 0.25 T, ▼; 1.0 T, ▲; and 5.0 T, ●.

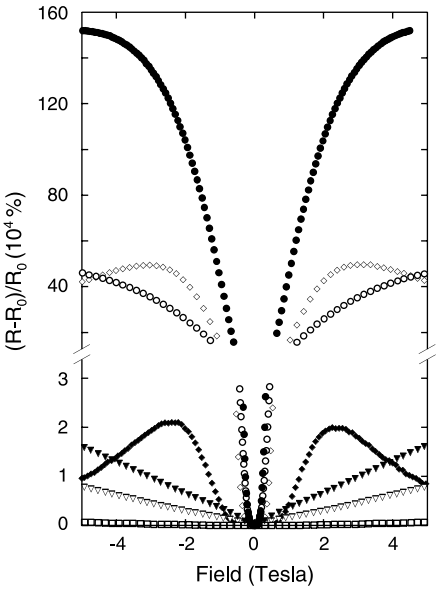

Fig. 3. The RT, high-field MR of a composite vdP disk of InSb and Au. The symbols correspond to the same values of α as specified in the caption of Fig. 1.

partially negated by the higher MR and higher ρ of the geometric MR sensor. Furthermore, physical MR information storage sensors such as spin-valve read heads may not provide sufficient sensitivity when scaled to sizes corresponding to the superparamagnetic limit for modern media of 100 Gb/inch^2, because of demagnetization and other magnetic effects (*22*). Composite nonmagnetic semiconductors with enhanced geometric MR $>$ ~100% at the relevant field (*23*), $H_{rel} = 0.05$ T, are not thus limited and could still exhibit high MR even when scaled to mesoscopic sizes (*24*). Also, their response time can be approximated by the inverse of the plasmon frequency, yielding a value in the subpicosecond range (*25*). This is substantially faster than the 10^{-9} to 10^{-10} s switching times of metallic sensors that are limited by magnetization dynamics (*22*). It should also be easy to provide the ~ 0.2 T self (*19*) or external biasing necessary to obtain a linear response and higher MR close to $H = 0$.

In addition to SNR, semiconductor physical MR sensors are often judged by a figure of merit $(1/R)(dR/dH)$ that typically exhibits a RT maximum of ~2.5 T^{-1} around a biasing field of 0.25 T (*2*). If we use this figure of merit, our MR sensor with $\alpha = 13/16$ reaches a corresponding maximum of 24 T^{-1} at 0.13 T, a factor of ~10 improvement, realized at a lower field. InSb enhanced geometric MR sensors should also be competitive with InSb Hall sensors (*3*) now produced in quantities $>10^9$/year for motors in consumer electronics.

Finally, one can readily anticipate sensors with still higher geometric MR values than reported in this proof-of-principle study. With higher mobility films and more vertical inhomogeneity side walls, we believe a further improvement of a factor of 2 to 3 of the MR to be in comfortable reach. In addition, the simple vdP geometry may not be optimal. Whatever the ultimate magnitude of achievable MR, it is clear that careful design of simple composite metal-semiconductor structures can result in sensors with substantially enhanced RT geometric MR.

References and Notes

1. J. A. Brug, T. C. Anthony, J. H. Nickel, *MRS Bull.* **21**, 23 (1996).
2. J. P. Heremans, *Mat. Res. Soc. Symp. Proc.* **475**, 63 (1997).
3. N. Kuze and I. Shibasaki, *III-V's Rev.* **10**, 28 (1997).
4. H. H. Wieder, *Hall Generators and Magnetoresistors* (Pion, London, 1971).
5. R. S. Popovic, *Hall Effect Devices* (Hilger, Bristol, UK, 1991).
6. P. M. Levy, *Solid State Phys.* **47**, 367 (1994).
7. C. N. R. Rao and B. Raveau, Eds., *Colossal Magnetoresistance, Charge Ordering and Related Properties of Manganese Oxides* (World Scientific, Singapore, 1998).
8. W. F. Egelhoff Jr. *et al.*, *J. Appl. Phys.* **78**, 273 (1995).
9. S. Jin, M. McCormack, T. H. Tiefel, R. Ramesh, *J. Appl. Phys.* **76**, 6929 (1994).
10. T. Thio *et al.*, *Phys. Rev. B* **57**, 12239 (1998).
11. W. Zawadzki, *Adv. Phys.* **23**, 435 (1974).
12. C. Herring, *J. Appl. Phys.* **31**, 1939 (1960).
13. A. Y. Shik, *Electronic Properties of Inhomogeneous Semiconductors* (Gordon and Breach, Amsterdam, 1995).
14. H. Weiss and M. Wilhelm, *Z. Phys.* **176**, 399 (1963).
15. S. D. Parker *et al.*, *Semicond. Sci. Technol.* **4**, 663 (1989).
16. C. M. Wolfe, G. E. Stillman, J. A. Rossi, *J. Electrochem. Soc. Solid-State Sci. Technol.* **119**, 250 (1972).
17. S. P. S. Parkin, *Bull. Am. Phys. Soc.* **44**, 1555 (1999).
18. T. Thio and S. A. Solin, *Appl. Phys. Lett.* **72**, 3497 (1998).
19. S. A. Solin *et al.*, *Appl. Phys. Lett.* **69**, 4105 (1996).
20. S. A. Solin, T. Thio, D. R. Hines, T. Zhou, unpublished data.
21. H. Neal Bertram, *Theory of Magnetic Recording* (Cambridge Univ. Press, Cambridge, 1994).
22. K. O'Grady, R. L. White, P. J. Grundy, *J. Magn. Magn. Mater.* **177–181**, 886 (1998).
23. The relevant field is the field that the sensor can access for a given read-head design with modern disk media.
24. For mesoscopic devices such as 100 Gb/inch^2 read-head sensors, we would use structures with lateral dimensions of order $L \sim 100$ nm and thickness of 30 nm. Such structures with $\alpha = 13/16$ would have an effective resistance of order 1 to 2 ohm for $0 < H <$ 0.05 T. Because this resistance is $\ll h/e^2$, where h is Planck's constant, conductance fluctuations should not impact the geometric MR. However, μ_{app} scales with $\mu = e\tau/m^*$, where τ is the electron mean free scattering time and m^* is the effective mass. For sample dimensions $L > \lambda$, the mean free path, $\tau = \lambda/v_F$, where v_F is the Fermi velocity. But when $L < \lambda$, scattering at the boundary dominates and $\tau \sim L/v_F$, so μ_{app} will scale with L and the geometric MR will scale (down) with L^2. Fortunately, the same boundary scattering also gives rise to a geometric MR that increases with H (and is larger than that of bulk material) up to a field H_c above which the MR decreases with increasing H [see F. Rahman *et al.*, *Semicond. Sci. Technol.* **14**, 478 (1999)]. Here, H_c corresponds to a cyclotron diameter of order the device size. The fields of interest here for 100 Gb/inch^2 sensors are well below H_c. For the InSb studied here, $\lambda \sim 300$ nm so the above described mesoscopic effects will be important and worth investigating. We are now using state-of-the-art e-beam lithography to fabricate and study the properties of mesoscopic enhanced geometric MR sensors.
25. M. F. Hoyaux, *Solid State Plasmas* (Pion, London, 1970).

26. Part of the work by J.J.H. was performed at EMCORE, Somerset, NJ. We thank J. A. Giordmaine for stimulating our interest in this work and L. F. Cohen and B. Altshuler for several useful discussions. We also thank S. Schwed and M. W. Pelczynski (EMCORE) for assistance with sample preparation and processing.

1 June 2000; accepted 18 July 2000

Evidence for Superfluidity in Para-Hydrogen Clusters Inside Helium-4 Droplets at 0.15 Kelvin

Slava Grebenev,[1]* Boris Sartakov,[2] J. Peter Toennies,[1]† Andrei F. Vilesov[1]*

A linear carbonyl sulfide (OCS) molecule surrounded by 14 to 16 para-hydrogen (pH_2) molecules, or similar numbers of ortho-deuterium (oD_2) molecules, within large helium-4 (^{4}He) droplets and inside mixed ^{4}He/^{3}He droplets was investigated by infrared spectroscopy. In the pure ^{4}He droplets (0.38 kelvin), both systems exhibited spectral features that indicate the excitation of angular momentum around the OCS axis. In the colder ^{4}He/^{3}He droplets (0.15 kelvin), these features remained in the oD_2 cluster spectra but disappeared in the pH_2 spectra, indicating that the angular momentum is no longer excited. These results are consistent with the onset of superfluidity, thereby providing the first evidence for superfluidity in a liquid other than helium.

The helium liquids ^{4}He and ^{3}He are the only known substances that exhibit the phenomenon of superfluidity below transition temperatures $T_c = 2.18$ K and $T_c = 2.4 \times 10^{-3}$ K, respectively. Despite intensive theoretical and experimental efforts during the ~60 years since its discovery, this remarkable effect still eludes complete understanding (*1*). Thus, there is considerable interest in finding superfluidity in other substances, and this is one of the reasons for the great interest in the recently discovered phenomenon of Bose-Einstein condensation (BEC) in the alkali atom gases (*2*). In 1972, Ginzburg and Sobyanin (*3*) estimated the BEC temperature of the modification of hydrogen molecules with antiparallel spins on the two nuclei (i.e., para-H_2 or pH_2 molecules) to be $T_c = 6$ K. They used the formula

$$T_c = \frac{3.31\hbar^2}{g^{2/3} M k_B} n^{2/3} \quad (1)$$

[1]Max-Planck-Institut für Strömungsforschung, Bunsenstraβe 10, 37073 Göttingen, Germany. [2]General Physics Institute, Russian Academy of Sciences, 117942 Moscow, Russia.

*Present address: Ruhr-University Bochum, Physical Chemistry II, D-44780 Bochum, Germany.
†To whom correspondence should be addressed. E-mail: jtoenni@gwdg.de